

Journal of Materials Chemistry A

Accepted Manuscript



This is an *Accepted Manuscript*, which has been through the Royal Society of Chemistry peer review process and has been accepted for publication.

Accepted Manuscripts are published online shortly after acceptance, before technical editing, formatting and proof reading. Using this free service, authors can make their results available to the community, in citable form, before we publish the edited article. We will replace this *Accepted Manuscript* with the edited and formatted *Advance Article* as soon as it is available.

You can find more information about *Accepted Manuscripts* in the [Information for Authors](#).

Please note that technical editing may introduce minor changes to the text and/or graphics, which may alter content. The journal's standard [Terms & Conditions](#) and the [Ethical guidelines](#) still apply. In no event shall the Royal Society of Chemistry be held responsible for any errors or omissions in this *Accepted Manuscript* or any consequences arising from the use of any information it contains.

Cite this: DOI: 10.1039/c0xx00000x

www.rsc.org/xxxxxx

Hierarchical structuring of metal-organic framework thin-films on quartz crystal microbalance (QCM) substrates for selective adsorption applications

Suttipong Wannapaiboon,^a Min Tu,^a Kenji Sumida,^b Kira Khaletskaya,^a Shuhei Furukawa,^b Susumu Kitagawa,^b and Roland A. Fischer^{*a}

Received (in XXX, XXX) Xth XXXXXXXXX 20XX, Accepted Xth XXXXXXXXX 20XX

DOI: 10.1039/b000000x

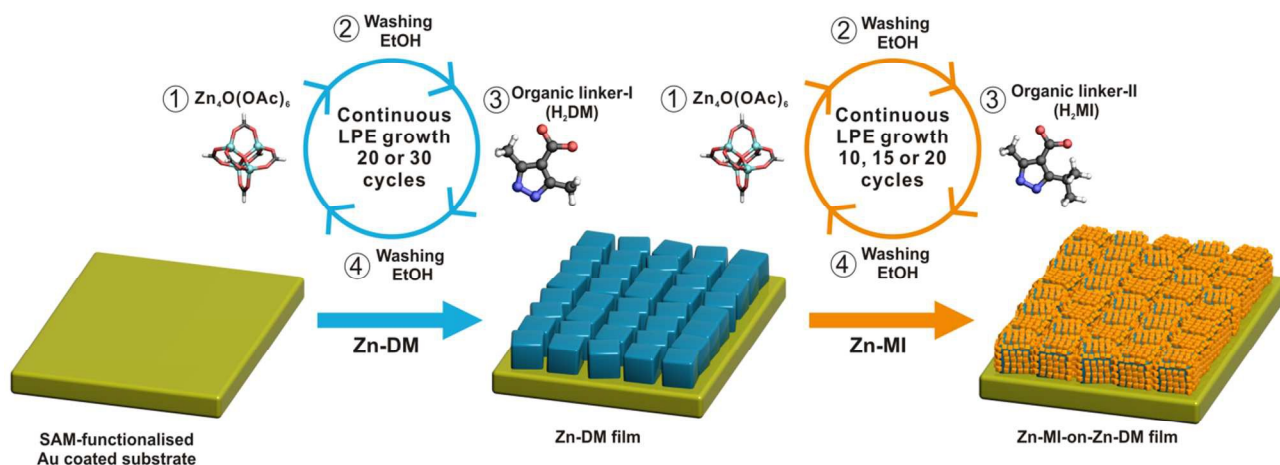
Continuous stepwise liquid-phase epitaxial (LPE) growth is one of the most effective procedures for structuring metal-organic frameworks (MOFs) as two-dimensional superstructures, such as thin-films. Alternation of the building block precursors between the individual LPE growth cycles (i.e. from one linker to the other) allows heterostructured MOF films consisting of two different MOFs with different structural or chemical properties to be synthesized with a precise control of the growth sequence. Here, we employ the LPE growth strategy for the preparation of highly functional, hierarchically structured core-shell architectures consisting of $[\text{Zn}_4\text{O}(\text{3,5-dialkylcarboxypyrazolate})_3]_n$ -based frameworks. Specifically, the small-pore $[\text{Zn}_4\text{O}(\text{3-methyl-5-isopropyl-4-carboxypyrazolate})_3]_n$ (**Zn-MI**) and $[\text{Zn}_4\text{O}(\text{3,5-diethyl-4-carboxypyrazolate})_3]_n$ (**Zn-DE**) frameworks are respectively deposited as a size selective layer upon larger-pore $[\text{Zn}_4\text{O}(\text{3,5-dimethyl-4-carboxypyrazolate})_3]_n$ (**Zn-DM**) and $[\text{Zn}_4\text{O}(\text{3-methyl-5-ethyl-4-carboxypyrazolate})_3]_n$ (**Zn-ME**) layers. Direct growth of the MOF layers on the Au surfaces of quartz crystal microbalance (QCM) sensors allowed the adsorption properties of the heterostructures to be probed in real-time. Multiple-component adsorption experiments in an environment-controlled QCM apparatus revealed size selectivity with respect to the adsorption of alcohols, as well as the molecular recognition of methanol over water. These properties stem from the positioning of the small-pore **Zn-MI** (or **Zn-DE**) layer on the larger-pore **Zn-DM** (or **Zn-ME**) layer, facilitating attractive synergistic properties for adsorptive selectivity and providing a possibility for further development in MOF-based sensing applications.

Introduction

Metal-organic frameworks (MOFs), or porous coordination polymers (PCPs), have been extensively investigated during the past decade. They are formed by coordination bonds between various kinds of metal centres (or inorganic clusters) and organic linkers¹, and provide well-defined crystalline networks that display a tremendous diversity in their chemical, structural, and dynamic properties.² The versatility in the range of precursor components that can be used at the molecular scale offers possibilities for precise manipulation of the framework structure as well as its associated properties.³ Hence, recent research has focused on rational design of the pore structure, size, shape and surface functionalities of MOFs in order to fine-tune and optimise the properties for real-world applications, ranging from gas storage, sensing, separation, and more recently, catalysis, bioreactors, and controlled drug release.⁴

In addition to tuning of the composition of MOFs, their physical form in the mesoscopic and macroscopic scales is known to uniquely affect their properties.^{5,6} The structuring of

MOFs in two-dimensional superstructures (e.g. thin films) is an emerging field that has received an increased attention over the last few years due to their potential use in membranes, coatings, QCM-based sensors and microcantilever-based sensors.⁷ Various methods have been developed to integrate MOF materials into devices by processing MOFs as thin films on various substrates^{8,9} and patterning them for specific applications.^{10,11} In particular, stepwise liquid-phase epitaxial (LPE) growth technique (also known as step-by-step deposition) is a potentially versatile method for preparing MOF thin films.^{12,13} In LPE fabrication, the substrate is alternately dosed with metal and organic precursor solutions⁹ leading to well-defined control of thickness, crystal size and orientation of the MOF constituting the thin film. The number of growth cycles and crystallization conditions can be fine-tuned such that the properties of the film are optimized for practical applications, including sensing, separation, catalysis, and as functional materials within electronic and optoelectronic devices.¹⁴



Scheme 1 Schematic illustration of the continuous stepwise liquid-phase epitaxial fabrication of heterostructured $[\text{Zn}_4\text{O}(\text{carboxypyrazolate})_3]_n$ thin films. Note that while a **Zn-MI-on-Zn-DM** heterostructure is used as an example, the other systems described in this work follow the same basic procedure. A SAM-functionalised Au-coated substrate is alternately exposed to solutions of $\text{Zn}_2\text{O}(\text{OAc})_6$ (Step 1) and 3,5-dimethyl-4-carboxypyrazole (H_2DM) (Step 3) with an intermediate EtOH washing step (Step 2 and 4) to induce a uniform film of **Zn-DM** (illustrated in blue colour). Then, the same procedure is repeated using 3-methyl-5-isopropyl-4-carboxypyrazole (H_2MI) to further grow a **Zn-MI** layer (illustrated in orange colour) on the original film, resulting in a **Zn-MI-on-Zn-DM** heterostructured film.

The hierarchical ordering of more than one MOF within a single, mesoscopic superstructure (as a so-called *heterostructure*) provides further opportunities to manipulate the characteristics of the system, particularly when a single MOF does not offer all required features for a specific application.¹⁵ Here, heteroepitaxial growth has been previously used for the deposition of one MOF onto another to produce various heterostructured systems, such as core-shell¹⁶ and sandwich (BAB-type) hybrid MOF crystals¹⁷. While most examples of such systems relate to single-crystal systems, this concept is in principle also applicable to thin films. Here, the stepwise LPE growth strategy is an attractive method for the fabrication of heterostructured MOF films, since the precursors can be switched between those for different MOFs during the film formation process.^{18,19} Using this method, several structurally-related MOFs,^{18–20} and even some MOFs with significantly mismatched lattice parameters²¹ and incompatible network structures²² have been prepared with a precise spatial control via an appropriate programming of the sequence and cycling frequency of the deposition process. In the case of two MOFs possessing different pore properties, the spatial control can lead to enhanced characteristics compared to a simple physical mixture of the same frameworks. For example, selective post-synthetic modification of heterostructured layer-pillared surface-mounted MOFs at an outer layer containing amino groups facilitated selective adsorption and diffusion of only certain components (such as hexane over cyclohexane and methanol over hexane) into the inner layer.^{23,24} Using a similar concept, incorporation of photoswitchable pendant groups, such as azobenzene, into the outer layer of a film was demonstrated as a pathway to control the adsorption permeability by light irradiation.²⁵

Despite this emerging interest in heterostructured MOF thin-films, fundamental investigations into their adsorptive properties still remains limited to a small number of systems, and the versatility of the LPE growth technique for the fabrication of

heterostructured systems is currently not well established. In order to advance both these aspects, we have selected the robust $[\text{Zn}_4\text{O}(\text{carboxypyrazolate})_3]_n$ -based series of MOFs,²⁶ for which the stepwise LPE method has been previously used (in both static batch-wise immersion¹³ and a continuous flow mode) to generate pure (single-phase) thin-films of the MOFs.²⁷ The single-phase thin-films could be readily integrated with quartz crystal microbalance (QCM) technologies for real-time monitoring of film growth, suggesting that similar observations will be possible for the heterostructured MOF films. Thus, we herein report the fabrication of heterostructured $[\text{Zn}_4\text{O}(\text{carboxypyrazolate})_3]_n$ MOF films, with an object of achieving high adsorption selectivity via rational selection of the positioning of the isostructures (Scheme 1). In particular, the small-pore $[\text{Zn}_4\text{O}(3\text{-methyl-5-isopropyl-4-carboxypyrazolate})_3]_n$ (**Zn-MI**) and $[\text{Zn}_4\text{O}(3,5\text{-diethyl-4-carboxypyrazolate})_3]_n$ (**Zn-DE**) frameworks are respectively deposited as a size selective layer upon larger-pore $[\text{Zn}_4\text{O}(3,5\text{-dimethyl-4-carboxypyrazolate})_3]_n$ (**Zn-DM**) and $[\text{Zn}_4\text{O}(3\text{-methyl-5-ethyl-4-carboxypyrazolate})_3]_n$ (**Zn-ME**) layers (The molecular structures of the organic linkers used for fabricating the heterostructured films are shown in Table S1.). The growth of a MOF with smaller pore openings as a shell layer is shown to provide adsorptive selectivity, while the presence of a larger-pore MOF as a core layer provides a high storage capacity of guest molecules. A systematic optimisation of the LPE fabrication process (i.e. number of fabrication cycles for each individual MOF component) is performed in order to obtain well-defined core-shell architectures of the heterostructured films that provide a high adsorptive selectivity with respect to alcohols of varying molecular size, as well as in the molecular recognition of methanol over water.

Experimental Section

Synthetic Procedures

The starting materials were synthesised using a procedure described previously.^{13,27} Basic zinc acetate ($\text{Zn}_4\text{O}(\text{OAc})_6$) was obtained by the sublimation of zinc acetate dihydrate ($\text{Zn}(\text{OAc})_2 \cdot 2\text{H}_2\text{O}$) at 280 °C under vacuum and was used as a pre-formed secondary building unit (SBU) metal precursor. The organic linkers 3,5-dimethyl-4-carboxypyrazole (H_2DM), 3-methyl-5-ethyl-4-carboxy pyrazole (H_2ME), 3-methyl-5-isopropyl-4-carboxypyrazole (H_2MI) and 3,5-diethyl-4-carboxypyrazole (H_2DE) were synthesised in three steps (Scheme S1). Firstly, the diketo-compound was synthesised by the acylation of alkyl acetoacetate with alkyl acid chloride. Then the cyclisation with hydrazine was performed to create the pyrazolate ring. Finally, the substituted ester group on the pyrazole was acidified to form the desired carboxypyrazolate linker.

15 Fabrication of heterostructured MOF thin films

Commercial Au-coated quartz crystal microbalances (QCM, Q-Sense, diameter 14 mm, thickness 0.3 mm, AT cut, fundamental frequency 4.95 MHz) were used as the substrates. Firstly, the surfaces of the substrates were -COOH terminated by a self-assembled monolayer (SAM) of 16-mercaptohexadecanoic acid (MHDA) by immersion in a 20 μM solution of MHDA in ethanol and 5% v/v acetic acid for 24 hours. The precursor solutions were freshly prepared for each fabrication, using a solution of basic zinc acetate (1.0 mM) in ethanol, and the carboxypyrazolate linker (0.5 mM) in a 4:1 v/v ethanol/water mixture. The MOF thin films were fabricated by stepwise liquid phase epitaxial (LPE) growth at 40 °C using the automated QCM instrument (Q-Sense E4 Auto) operated in a continuous flow mode with a flow rate of 100 $\mu\text{L min}^{-1}$. Generally, the precursor solutions were alternately dosed to the QCM deposition cell, each for 10 min. In between each precursor dosing, a washing step (ethanol) was carried out for 5 min. Note that in the following description, one deposition cycle represents exposure of the functionalised QCM substrate to basic zinc acetate (10 min), ethanol (5 min), carboxypyrazolate linker (10 min) and ethanol (5 min).

Three different types of the shell-on-core heterostructured films were produced: **Zn-MI-on-Zn-DM**, **Zn-DE-on-Zn-DM** and **Zn-MI-on-Zn-ME** (see the summary in Table S1 in the supplementary information). The number of deposition cycles of each individual MOF component was varied from 10 to 30 cycles. In the following discussion, we employ the notation “MOF(*x*)-on-MOF(*y*)”, where *x* and *y* represent the number of deposition cycles carried out in forming the shell and core MOFs, respectively. For example, **Zn-MI(20)-on-Zn-DM(20)** heterostructured film refers to a sample in which **Zn-DM** is fabricated for 20 cycles on a functionalised QCM substrate, followed by **Zn-MI** for 20 cycles (see Scheme 1). During thin-film fabrication, the change in QCM frequency was recorded in-situ in order to monitor the film growth.

50 Characterisation

Phase purity of basic zinc acetate were characterised by powder X-ray diffraction (XRD) using an X'Pert PanAnalytical equipment (Bragg-Brentano geometry, Cu K_α radiation, 2 θ from 5° to 50°, position sensitive detector). The organic linkers were identified by nuclear magnetic resonance (NMR) spectroscopy using a Bruker Advance DPX 200 spectrometer (automatic and routine settings). The two-dimensional grazing incidence X-ray

diffraction (2D-GIXRD) data of the obtained thin films were collected at Beamline 9 at DELTA Synchrotron, Germany (X-ray beam with energy of 12.38 keV or wavelength of 1.001 Å, sample-to-detector distance of 500 mm and the incidence angle of 0.6°). The crystalline phase of the MOF thin films was determined by the out-of-plane cuts of the 2D-GIXRD patterns. Infrared Reflection Absorption Spectra (IRRAS) of the activated MOF thin films were recorded by a Bruker Alpha-P FTIR instrument (using the external reflection modules) inside a glovebox. Surface morphology and surface coverage of the MOF films were investigated by a field emission scanning electron microscope (FESEM, LEO (Zeiss) 1530 Gemini FESEM) and an environmental scanning electron microscope (ESEM, FEI ESEM Dual Beam™ Quanta 3D FEG). Prior to the SEM measurements, the samples were coated with carbon in order to increase the conductivity before loading into the instrument.

Organic vapour adsorption measurements

The sorption properties of the heterostructured MOF thin films were studied by an environmental-controlled quartz crystal microbalance (BEL-QCM-4 equipment, BEL Japan) equipped with two vaporisers for different volatile organic compounds (VOCs) with their own set of mass flow controllers. Herein, two alcohols (methanol and isopropanol) as well as water were selected as probe volatile compounds. Schematic representation of experimental setup for sorption experiments on MOF-deposited QCM substrates are shown in Fig. S2. All sorption experiments were carried out at 25 °C. The samples were activated prior to the sorption experiments by immersion in dichloromethane for 24 h (exchanging molecules within the pores) followed by drying under an argon stream. Then, the samples were heated in the BEL-QCM instrument at 70 °C under a dry helium gas flow (100 sccm) for 2 h until the QCM frequency was stable (± 5 Hz over 20 min). The mass of the deposited MOF thin film was calculated by the difference in the fundamental QCM oscillation frequency and the frequency after final activation of the sample. Single-component adsorption isotherms of each probe compound were collected using a single vaporiser. The desired relative vapour pressure (P/P_0) of saturated organic vapour in helium gas was varied between 0.0~95.0%, and the specific adsorption amount was calculated from the observed QCM frequency according to the Sauerbrey equation (see supplementary information).²⁸ For mixed-component adsorption data, the experiments were performed using two different probe compounds. Here, the P/P_0 of one probe compound was kept constant at a certain amount (maximum 45% P/P_0), while the other was varied between 0~45% P/P_0 . The total gas flow through the system was fixed at 100 sccm, with mixing of the two components in the manifold prior to exposure to the QCM cell (see Fig. S2).

Results and discussion

Stepwise LPE growth is an attractive method of introducing the concepts of heterostructured bulk MOFs to thin films via sequential and controlled deposition cycles of the metal and organic precursors to the substrate.¹⁸ The precursors can be changed at any time (to introduce a functionalised analogue of an organic linker for example) during the thin film fabrication at a

pre-programmed point to induce growth of other MOFs on a pre-deposited parent MOF film. However, the range of MOFs that have been processed via the LPE method is very limited, and warrants further studies to understand its versatility. In the best-known example, heterostructured films of the layer-pillared surface-mounted MOFs (SURMOFs)^{18–20} were epitaxially grown, wherein an amino-functionalised $[\text{Cu}_2(\text{NH}_2\text{-bdc})_2(\text{dabco})]_n$ layer was deposited on an unfunctionalised $[\text{Cu}_2(\text{bdc})_2(\text{dabco})]_n$ or $[\text{Cu}_2(\text{ndc})_2(\text{dabco})]_n$ inner layer ($\text{NH}_2\text{-bdc}$ = 2-amino-benzene-1,4-dicarboxylate, bdc = benzene-1,4-dicarboxylate, ndc = naphthalene-1,4-dicarboxylate, and dabco = 1,4-diazabicyclo-(2.2.2)-octane).^{20,23,24} Here, size-based adsorption permeability was demonstrated via post-synthetic modification of the amino-containing SURMOF outer layer.^{23,24} However, the films were not chemically robust (particularly in the presence of moisture), limiting their potential for practical uses under ambient conditions.¹⁰ This has prompted investigations of a similar type in the context of other more stable materials that could be amenable for use under biologically or industrially relevant conditions.

In this work, we selected the more chemically robust $[\text{Zn}_4\text{O}(\text{3,5-dimethyl-4-carboxypyrazolate})_3]_n$ (**Zn-DM**) and its 3,5-dialkyl substituted analogues for fabrication as heterostructured MOF thin-films on QCM substrates by LPE method. Based on our previous work, the formation of thin-films of **Zn-DM** and its isostructural thin films was proposed to occur via an island growth mode during the nucleation stage, followed by an overgrowth of the pre-formed MOF crystallites to form dense MOF films. Therefore, we surmised that heterostructured thin-films could be formed with a variety of isostructural compounds in a core-shell architecture.²⁷ Herein, the LPE fabrication process is optimised to achieve a well-controlled hierarchical arrangement of individual MOF components within heterostructured films. The performance of these films in the context of selective adsorption properties are then systematically investigated using a QCM apparatus, demonstrating unique properties stemming from the nature of the structuring.

Synthesis and characterisation of heterostructured thin-films

The heterostructured $[\text{Zn}_4\text{O}(\text{carboxypyrazolate})_3]_n$ MOF thin-films were fabricated at 40 °C by the stepwise LPE method in the continuous mode using a procedure based on a previously described method.²⁷ Here, two $[\text{Zn}_4\text{O}(\text{1,3-dialkyl-4-carboxypyrazolate})_3]_n$ isostructural compounds with different pore apertures and volumes were integrated by firstly fabricating the larger-pore MOF (**Zn-DM** or **Zn-ME**) on the carboxylate-terminated QCM substrate. Then, the smaller-pore MOF (**Zn-MI** or **Zn-DE**) was fabricated thereon, leading to the formation of the heterostructured MOF film (Scheme 1).

During the fabrication procedure, the QCM frequency change (which is proportional to the mass uptake on QCM substrate) was monitored. The temporal frequency change during growth for **Zn-MI-on-Zn-DM** films using various deposition cycle counts for each component are presented in Fig. S3. The overall mass of the respective MOF components linearly increases with the number of deposition cycles. However, the change in the rate of frequency change upon switching the linker suggests that the growth rate of the **Zn-DM** inner layer is significantly higher than that of the **Zn-MI** outer layer, presumably due to the different growth behaviour of the two MOFs.^{27, 29}

The crystallinity of the heterostructured MOF thin films was characterised by grazing incidence X-ray diffraction (GIXRD) using a synchrotron X-ray source ($\lambda = 1.00130 \text{ \AA}$). The out-of-plane cuts of the obtained GIXRD patterns for different compositions of the **Zn-MI-on-Zn-DM** thin-films are shown in Fig. 1 (the corresponding data for the **Zn-MI-on-Zn-ME** and **Zn-DE-on-Zn-DM** systems are also displayed in Fig. S5). These data indicate the formation of highly-crystalline films with a preferential orientation in the [100] direction, corresponding with the attachment of the crystallites to the substrate via one of their cubic facets. The isostructural nature of the two components within the heterostructured films (and almost identical unit cell dimensions²⁷; **Zn-DM**: $a = 20.036 \text{ \AA}$, **Zn-MI**: $a = 20.150 \text{ \AA}$) leads to just a single set of peaks that are well-matched with the diffraction peak positions for the pure **Zn-DM** material.

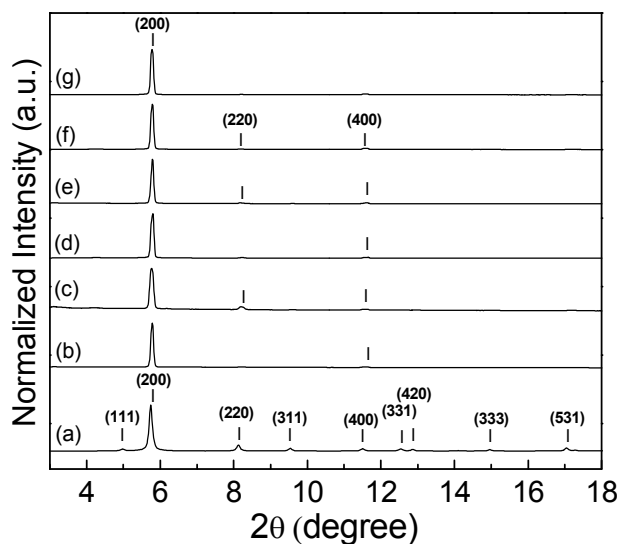


Fig. 1 (a) Simulated powder X-ray diffraction pattern for bulk **Zn-DM** ($\lambda = 1.00130 \text{ \AA}$); and out-of-plane cuts from 2D-grazing incidence X-ray diffraction (GIXRD) patterns using a synchrotron source ($\lambda = 1.00130 \text{ \AA}$) for (b) **Zn-MI(10)-on-Zn-DM(20)**, (c) **Zn-MI(15)-on-Zn-DM(20)**, (d) **Zn-MI(20)-on-Zn-DM(20)**, (e) **Zn-MI(10)-on-Zn-DM(30)**, (f) **Zn-MI(15)-on-Zn-DM(30)**, and (g) **Zn-MI(20)-on-Zn-DM(30)**. The numbers within the parentheses in the figure indicate the Miller indices of the crystal planes.

In order to demonstrate the presence of both MOF components, infrared reflection absorption spectra (IRRAS) were collected for the heterostructured films (Fig. S6 to S8). While the transmittance bands belonging to both components (grey bands) are observed at the same frequencies in both the homostructured and heterostructured films, the bands characteristic to each MOF component (blue and yellow bands) are synergistically presented in the heterostructured films (see Fig. S7 for the data corresponding to **Zn-DE-on-Zn-DM** films). Importantly, this data, taken together with the X-ray diffraction data described above, illustrate the formation of preferred oriented heterostructured films for each of the combination of MOF components surveyed in this work.

To obtain insight into the morphology and surface coverage of the heterostructured MOF films, the samples were characterised by SEM. Fig. 2 shows the scanning electron microscopy (SEM) images of surfaces of a pure **Zn-DM(20)** film (Fig. 2A),

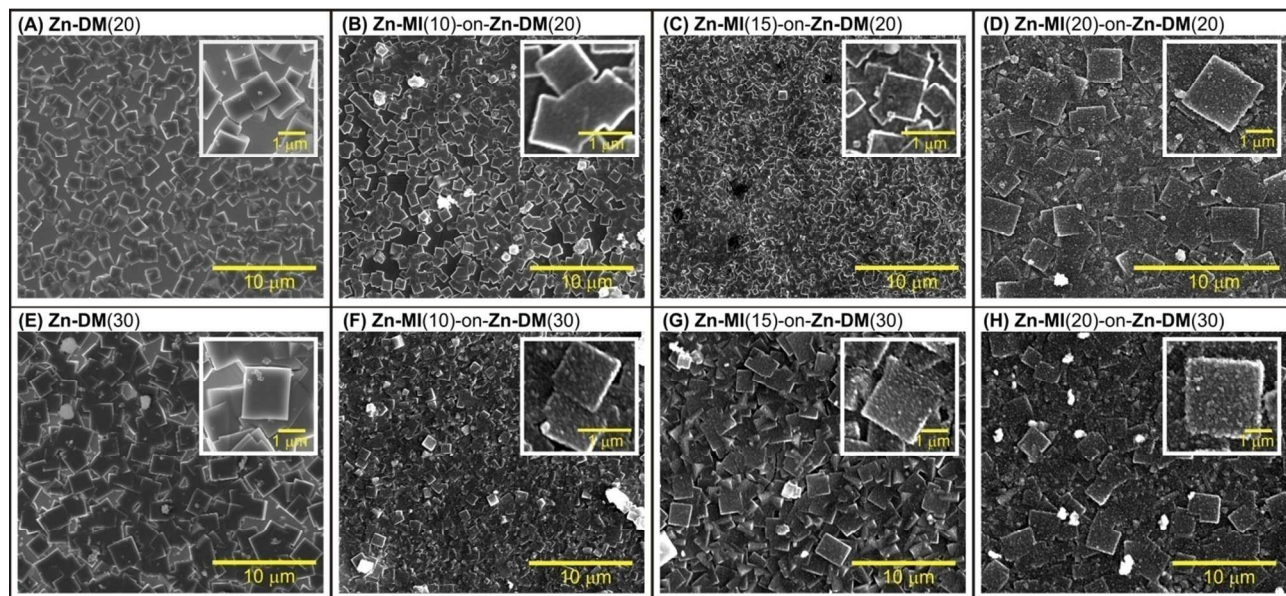


Fig. 2 Scanning electron microscopy (SEM) images of the surfaces of (A) a pure **Zn-DM(20)** film, (B)-(D) the corresponding **Zn-MI(x)-on-Zn-DM(20)** heterostructured films, (E) a pure **Zn-DM(30)** film, and (F)-(H) the corresponding **Zn-MI(x)-on-Zn-DM(30)** heterostructured films. Note that *x* represents the number of deposition cycles for **Zn-MI** component (10, 15 and 20 cycles).

Zn-MI(x)-on-Zn-DM(20) heterostructured films (Fig. 2B-D), a pure **Zn-DM(30)** film (Fig. 2E), and **Zn-MI(x)-on-Zn-DM(30)** heterostructured films (Fig. 2F-H). As can be understood from the images of the pure **Zn-DM** films (Fig. 2A and 2E), LPE fabrication leads to cubic crystallites that are anchored to the –COOH terminated surface via one of their facets. Increasing the number of growth cycles is shown to increase the crystal size, with the **Zn-DM(30)** film exhibiting a crystal size of approximately 2 μm and a greater surface coverage of the Au substrate.

For the heterostructured films, the size of the **Zn-MI** crystallites is significantly smaller than that of the **Zn-DM** particles, potentially due to the different growth behaviour of the two MOFs. As observed for pure films of the two compounds, while a greater number of LPE growth cycles leads growth of the **Zn-DM** into larger crystals, additional nucleation is more preferable in the case of **Zn-MI**. This leads to the formation of a large number of **Zn-MI** nanocrystals, which is corroborated by the **Zn-MI-on-Zn-DM** heterostructured films exhibiting rougher surfaces due to the attachment of the **Zn-MI** nanocrystals to the smooth facets of the cubic **Zn-DM** crystallites in a core-shell fashion.

The number of LPE fabrication cycles required to achieve a dense surface coverage of the thin-film on the substrate, and a fully-covered shell-on-core heterostructure, was optimised for the respective MOF components. While a **Zn-MI(10)-on-Zn-DM(20)** sample did not afford full surface coverage of the MOF film (Fig. 2B), increasing the number of shell-component **Zn-MI** fabrication cycles to at least 15 cycles (Fig. 2C and 2D) and/or increasing the core-component **Zn-DM** fabrication cycles to 30 cycles (Fig. 2F to 2H) gave enhanced surface coverage. Note that the **Zn-MI-on-Zn-ME** and **Zn-DE-on-Zn-DM** systems show similar characteristics as probed by SEM (see Fig. S9). The cross-sectional SEM images of the **Zn-MI-on-Zn-DM** films (Fig. S10)

indicate the formation of dense MOF thin films on the functionalised Au-coated QCM substrate, except in the case of the **Zn-MI(10)-on-Zn-DM(20)** film, for which full surface coverage was not observed as mentioned above. These data suggest that the $[\text{Zn}_4\text{O}(\text{carboxypyrazolate})_3]_n$ films are formed by the overgrowth of the island MOF nuclei in a core-shell fashion, with further intergrowth to form dense films.

Sorption properties of heterostructured MOF thin films

Next, the adsorption properties of the heterostructured MOF films were probed using alcohol molecules of different kinetic diameter (i.e. methanol: 3.6 Å; isopropanol: 4.7 Å), and water. As described below, both single- and multiple-component adsorption experiments were carried out to characterise the storage capacity of the films and the possibility for selective adsorption applications.

1. Single-component alcohol adsorption

The single-component alcohol adsorption data collected at 25 °C for the **Zn-MI-on-Zn-DM** heterostructured films and their pure counterparts are presented in Fig. 3 (with the corresponding data for **Zn-DE-on-Zn-DM** and **Zn-MI-on-Zn-ME** films are displayed in Fig. S11 and S12, respectively). The methanol adsorption data for the **Zn-MI-on-Zn-DM** heterostructured films exhibit a Type-I isotherm typical of a microporous solid in a similar manner to the pure **Zn-DM** film (see Fig. 3A). Here, the normalised total methanol adsorption capacity (quantity of methanol per gram of MOF component) is greatest for the pure **Zn-DM** film, and decreases as the proportion of **Zn-MI** increases in the heterostructured films. This is due to the lower surface area of **Zn-MI** (BET surface area 200 m² g⁻¹) compared to **Zn-DM** (BET surface area 640 m² g⁻¹) resulting from the bulkier alkyl chains present in the organic linker.²⁷ Most notably, increasing the number of **Zn-DM** fabrication cycles from 20 to 30 leads to a significant increase in the methanol adsorption capacity when the

number of **Zn-MI** cycles is held constant (i.e. when y is increased, but x remains unchanged). Note that, based on the in-situ QCM frequency changes (Fig. S3), the total composition of the heterostructured MOF film is dominated by the DM core component. Moreover, the **Zn-DM(30)** film features a well-defined morphology and high crystallinity, which is also likely of benefit to the adsorption capacity. Similar trends were observed for the methanol adsorptions within the **Zn-DE-on-Zn-DM** (Fig. S11A) and **Zn-MI-on-Zn-ME** (Fig. S12A) heterostructured films, wherein the adsorption predominantly arises from the highly-crystalline **Zn-DM** and **Zn-ME** core components, respectively.³⁰

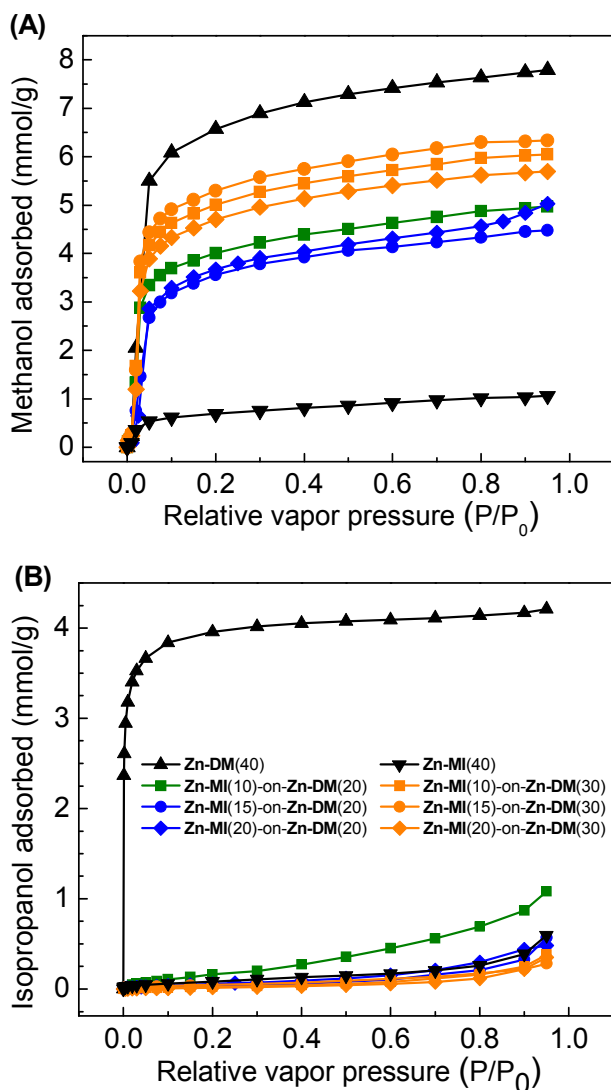


Fig. 3 Single-component (A) methanol and (B) isopropanol adsorption isotherms at 25 °C for **Zn-MI**(x)-on-**Zn-DM**(y) heterostructured films and **Zn-MI** and **Zn-DM** recorded using an environmental-controlled QCM. Note that x and y represents the number of deposition cycles for **Zn-MI** and **Zn-DM**, respectively.

The isopropanol adsorption isotherms (Fig. 3B) were collected for the same set of samples at 25 °C (the corresponding data for the **Zn-DE-on-Zn-DM** and **Zn-MI-on-Zn-ME** films are displayed in S11B and S12B, respectively). Here, it is clearly

observed that isopropanol, which features a larger molecular diameter, is adsorbed inside the pores of the pure **Zn-DM** (or **Zn-ME**, see Fig. S12B) film, but not in the pure **Zn-MI** (or **Zn-DE** see Fig. S11B) film. In the heterostructured films, there is also no significant uptake of isopropanol upon formation of the smaller-pore shell layer, except at the lowest coverage of **Zn-MI(10)-on-Zn-DM(20)** (adsorption curves labelled in green in Fig. 3). This can be attributed to a fully-covered shell-on-core structure at higher coverages, as evidenced by the SEM data, which achieves exclusion of isopropanol from the core **Zn-DM** layer. At lower coverages, diffusion pathways still exist to the core layer, which is not desired from the viewpoint of obtaining a size-based selective adsorption profile. Optimisation of the number of fabrication cycles for the **Zn-DM** and **Zn-MI** components revealed that at least 15 **Zn-MI** fabrication cycles are required for complete coverage of the **Zn-DM** layer formed by a 20- or 30-cycle fabrication process.

From the perspective of achieving selective adsorption properties, all of the films featuring a sufficient coverage of **Zn-MI** as the shell layer display size-selective adsorption of methanol over isopropanol. This can be ascribed to the small pore apertures of **Zn-MI**, which inhibit access of the isopropanol to the **Zn-DM** phase. Meanwhile, although the adsorption capacity of a **Zn-MI(40)** displays a small (< 1 mmol/g) uptake for methanol, the pores are sufficiently large to facilitate diffusion of the molecules through its pores to the higher-capacity **Zn-DM** phase. Hence, controlled hierarchical structuring that integrates the two MOFs is crucial not only for achieving selective adsorption, but also for increasing the total adsorption capacity of the system. In other words, the smaller-pore **Zn-MI** (or **Zn-DE**) shell layer contributes toward the adsorption selectivity, while the larger-pore **Zn-DM** (or **Zn-ME**) core layer plays a dominant role in dictating the total adsorption capacity.

2. Multiple-component adsorption

2.1 Size-selective adsorption of alcohols

The size-based adsorptive selectivity of the films was further examined via multiple-component adsorptions experiments using methanol and isopropanol as adsorbates. Here, all whole adsorption experiments were performed at 25 °C with a fixed total gas flow of 100 sccm. In a typical experiment, the composition of one of the alcohols was kept constant (either 30% or 45% P/P_0), while the quantity of the other was varied in a range from 0 to 45% P/P_0 . The streams of the two probe compounds were mixed in a dedicated manifold prior to being introduced into the QCM sample cell, and the adsorption quantities were computed after stabilisation of the oscillation frequency.

The comparison between the multiple-component adsorption data and the corresponding single-component (methanol and isopropanol) adsorption data are shown in Fig. 4 for a **Zn-MI(20)-on-Zn-DM(20)** film (see Fig. S13-S23 for corresponding data for other film compositions). An experiment performed under a variable methanol concentration (varied P/P_0 from 0-45%) in the presence of 30% and 45% P/P_0 isopropanol concentration (blue and orange plots in Fig. 4A), revealed a mass uptake profile almost indistinguishable from that of the single-

component methanol adsorption isotherm (black plot in Fig. 4A). This suggests that the pores are free from adsorbed molecules under the original isopropanol flow, and only methanol molecules are adsorbed as its concentration is increased.³¹ In contrast, the analogous experiment using a variable isopropanol adsorption in the presence of a constant 45% methanol concentration shows a large uptake of approximately 0.13 g/g prior to the introduction of isopropanol. Subsequent introduction of isopropanol to the 45% concentration of methanol leads to little additional uptake (see green plot, Fig. 4B). This nearly constant total adsorption amount is approximately equal to the total adsorption amount at 45% methanol concentration in the single-component methanol adsorption isotherm. This suggests that the isopropanol permeation into the MOF film is blocked by the **Zn-MI** shell component. Based on these data, it can be directly concluded that the **Zn-MI(20)-on-Zn-DM(20)** heterostructured film exhibits selective adsorption of methanol over isopropanol even under mixed component conditions.

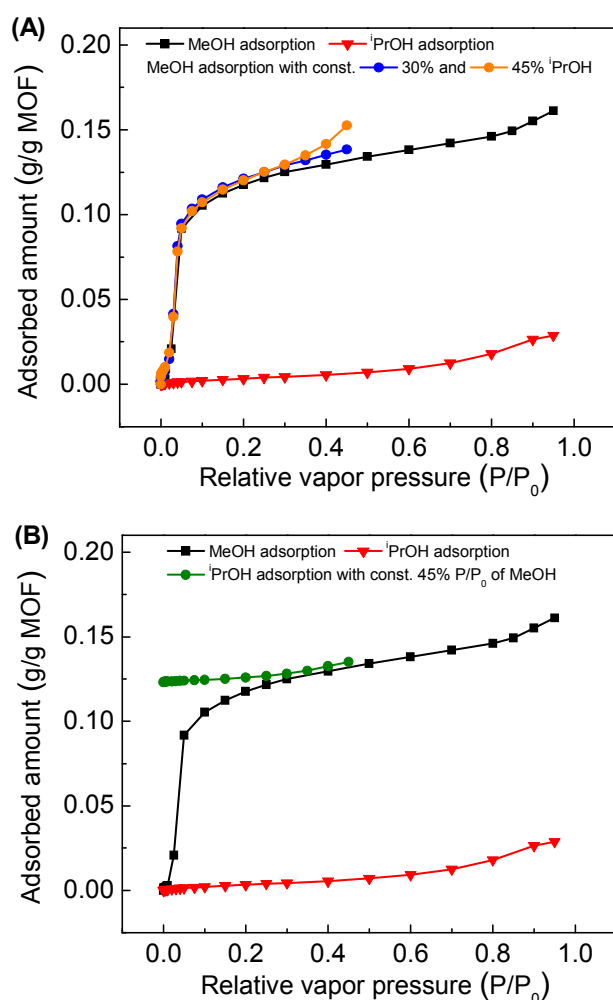


Fig. 4 Methanol/isopropanol single- and multi-component adsorption at 25 °C for a heterostructured **Zn-MI(20)-on-Zn-DM(20)** film. The individual plots represent (A) variable methanol concentration in the presence of an isopropanol concentration of 30% (blue) and 45% (orange); (B) variable isopropanol adsorption in the presence of a methanol concentration of 45% (green). In both plots, the single-component methanol (black) and isopropanol (red) adsorption isotherms for the same sample are included for reference.

In the cases of the **Zn-MI(10)-on-Zn-DM(20)** (Fig. S13) and **Zn-DE(10)-on-Zn-DM(20)** (Fig. S18) films, the multi-component adsorption curve for a variable methanol concentration under a fixed 30% concentration isopropanol shows a substantial deviation from the single-component methanol adsorption curve. The higher total adsorption capacity can be ascribed to both methanol and isopropanol molecules being adsorbed in these two heterostructured MOF films. This confirms the presence of just a partial shell-on-core ordering within these films, which allow isopropanol molecules to permeate into the MOF film via regions where **Zn-DM** is exposed, leading to the limited adsorption selectivity. This also further emphasises the importance of optimising the number of LPE fabrication cycles for each MOF component in order to obtain a fully heterostructured film.

2.2 Molecular recognition of methanol over water

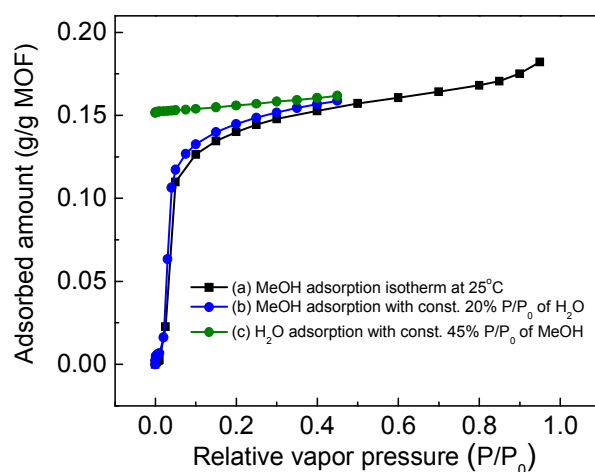


Fig. 5 Methanol and methanol/water multi-component mass uptake profiles recorded at 25 °C for a heterostructured **Zn-MI(20)-on-Zn-DM(30)** film. The individual plots represent (a) a single-component methanol adsorption isotherm, (b) variable methanol concentration in the presence of a 20% water concentration (blue); and (c) variable water concentration in the presence of a 45% methanol concentration (green).

The multiple-component QCM apparatus was also employed to test the methanol/water selectivity of the films. In a similar manner to the methanol/isopropanol mixed component experiments described above, the films were tested by varying the concentration of one of the components (methanol or water) under a fixed concentration of the other adsorbate. The multiple-component adsorption profile at 25 °C for a **Zn-MI(20)-on-Zn-DM(30)** film using a variable methanol concentration under a constant water vapour concentration of 20% is shown in Fig. 5 (blue plot, see Fig. S24 and S25 for other film compositions). Here, the heterostructured MOF film shows a similar isotherm shape and saturation adsorption capacity to the single-component methanol adsorption isotherm (black plot). In contrast, when the water vapour concentration is varied under a constant methanol concentration of 45% (green plot), a large mass increase is observed prior to the introduction of water vapour. Increasing the concentration of water vapour from 0% to 45% under these conditions does not provide a significant increase in the total uptake. This lack of permeation of water molecules into the films is surprising, although the kinetic diameter of water (2.6 Å) is

smaller in comparison with methanol (3.6 Å). This observation could be rationalised due to the hydrophobicity of the frameworks, which prevents water from being adsorbed within the pores, providing adsorptive selectivity toward methanol molecules. This suggests that in addition to the size-based (kinetic) selectivity observed for the alcohols, the films also possess an adsorptive selectivity based on a molecular recognition mechanism. Thus, from a practical perspective, these heterostructured MOF films coupled with QCM sensors can be used for selective adsorption of alcohol vapours even in the presence of relatively high levels of humidity. This concept of hierarchically structuring MOF thin films could provide possibilities for further development in MOF-based sensing applications via control over specific responses to certain probe molecules facilitated by selective adsorption.

Conclusions

The effective continuous stepwise LPE growth procedure is used for hierarchically structuring MOF materials as thin films on QCM sensors. A specific spatially-controlled ordering of two structurally-related $[\text{Zn}_4\text{O}(\text{carboxypyrazolate})_3]_n$ -based MOF thin films with different pore features in a core-shell fashion, which combines the MOF with smaller pore as a shell layer and larger pore as a core layer, reveals promising selective adsorption properties. Optimisation of the number of LPE fabrication cycles for each individual MOF component is required to achieve a full coverage of the MOF shell layer on the pre-deposited core MOF layer. In the heterostructured films studied here, the smaller-pore **Zn-MI** and **Zn-DE** shell components demonstrate size-based selectivity, while the **Zn-DM** and **Zn-ME** core components significantly dictate the overall adsorption capacity. Hence, the size-selective adsorptions of alcohols as well as the molecular recognition of alcohol over water can both be achieved by these heterostructured MOF thin-films. The excellent adsorptive selectivity and high storage capacity combined with a high robustness toward moisture presents these heterostructured $[\text{Zn}_4\text{O}(\text{carboxypyrazolate})_3]_n$ thin films as a promising candidate for practical use in MOF-based devices. For widespread industrial use, greater control over the uniformity of the MOF thin film on larger substrates (as well as spatial localisation of the MOF film to small working units within specific devices), as well as investigations directed toward understanding the mechanical stability will provide an additional perspective toward developing these materials within next-generation devices.

Acknowledgements

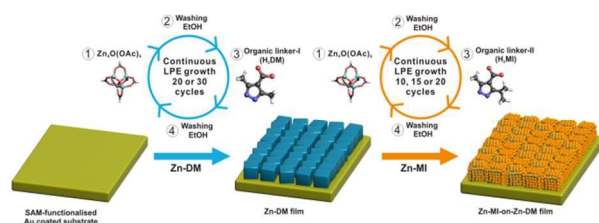
This work was started within the Priority Program 1362 “Metal-Organic Frameworks” and further supported by the Cluster of Excellence RESOLV (EXC 1069) funded by the Deutsche Forschungsgemeinschaft (DFG). iCeMS is supported by the World Premier International Research Initiative (WPI), MEXT, Japan. DELTA is acknowledged for the grazing incidence X-ray diffraction measurements at BL09. S.W. is grateful for a PhD scholarship from the Royal Thai Government under the Ministry of Science and Technology as well as the International Research Budget (IRB) funding from Research School, Ruhr-University Bochum (GSC 98). M.T is grateful for a PhD fellowship from the China Scholarship Council (CSC). K.S. is grateful to the JSPS Postdoctoral Fellowship Program for Foreign Researchers. Dr.

Christian Sternemann and Dr. Michael Paulus are acknowledged for their valuable guidance in the grazing incidence X-ray diffraction measurements at BL09, DELTA. Dr. Raghavender Medishetty is acknowledged for his valuable discussion and his support for scheme preparation.

Notes and references

- ^a Chair of Inorganic Chemistry II - Organometallics and Materials Chemistry, Ruhr-University Bochum, D-44780 Bochum, Germany. Fax: +49(0) 234-32-14174; Tel: +49(0) 234-32-23629; E-mail: roland.fischer@rub.de
- ^b Institute for Integrated Cell-Material Sciences (WPI-iCeMS), Kyoto University, Yoshida, Sakyo-ku, Kyoto 606-8501, Japan. Fax: +81(0) 75-753-9820; Tel: +81(0) 75-753-9868
- † Electronic Supplementary Information (ESI) available: [details of any supplementary information available should be included here]. See DOI: 10.1039/b000000x/
- a) O. M. Yaghi, M. O’Keeffe, N. W. Ockwig, H. K. Chae, M. Eddaoudi and J. Kim, *Nature*, 2003, **423**, 705–714; b) S. Kitagawa, R. Kitaura and S.-i. Noro, *Angew. Chem. Int. Ed.*, 2004, **43**, 2334–2375; c) G. Férey, C. Mellot-Draznieks, C. Serre and F. Millange, *Acc. Chem. Res.*, 2005, **38**, 217–225.
 - a) S. Horike, S. Shimomura and S. Kitagawa, *Nat Chem*, 2009, **1**, 695–704; b) G. Férey and C. Serre, *Chem. Soc. Rev.*, 2009, **38**, 1380–1399; c) K. Barthelet, J. Marrot, D. Riou and G. Férey, *Angew. Chem.*, 2002, **114**, 291–294.
 - a) H. Li, M. Eddaoudi, M. O’Keeffe and O. M. Yaghi, *Nature*, 1999, **402**, 276–279; b) G. Férey, *Chem. Soc. Rev.*, 2008, **37**, 191–214.
 - a) M. Dincă and J. R. Long, *Angewandte Chemie International Edition*, 2008, **47**, 6766–6779; b) M. D. Allendorf, R. J. T. Houk, L. Andruszkiewicz, A. A. Talin, J. Pikarsky, A. Choudhury, K. A. Gall and P. J. Hesketh, *J. Am. Chem. Soc.*, 2008, **130**, 14404–14405; c) B. Wang, A. P. Cote, H. Furukawa, M. O’Keeffe and O. M. Yaghi, *Nature*, 2008, **453**, 207–211; d) Metal Organic Frameworks Themed Issue, *Chem. Soc. Rev.*, 2009, **38**, 1201–1508; e) 2012 Metal Organic Frameworks Issue, *Chem. Rev.*, 2012, **112**, 673–1268; f) Metal-Organic Frameworks (MOFs), *Chem. Soc. Rev.*, 2014, **43**, 5415–6172.
 - a) E. A. Flugel, A. Ranft, F. Haase and B. V. Lotsch, *J. Mater. Chem.*, 2012, **22**, 10119–10133; b) Y. Sakata, S. Furukawa, M. Kondo, K. Hirai, N. Horike, Y. Takashima, H. Uehara, N. Louvain, M. Meilikhov, T. Tsuruoka, S. Isoda, W. Kosaka, O. Sakata and S. Kitagawa, *Science*, 2013, **339**, 193–196. c) K. Sumida, N. Moitra, J. Reboul, S. Fukumoto, K. Nakanishi, K. Kanamori, S. Furukawa and S. Kitagawa, *Chem. Sci.*, 2015, **6**, 5938–5946.
 - S. Furukawa, J. Reboul, S. Diring, K. Sumida and S. Kitagawa, *Chem. Soc. Rev.*, 2014, **43**, 5700–5734.
 - a) D. Zacher, O. Shekhah, C. Wöll and R. A. Fischer, *Chem. Soc. Rev.*, 2009, **38**, 1418–1429; b) O. Shekhah, J. Liu, R. A. Fischer and C. Wöll, *Chem. Soc. Rev.*, 2011, **40**, 1081–1106; c) A. Bétard and R. A. Fischer, *Chem. Rev.*, 2012, **112**, 1055–1083.
 - a) A. Schoedel, C. Scherb and T. Bein, *Angew. Chem. Int. Ed.*, 2010, **49**, 7225–7228; b) A. Huang, H. Bux, F. Steinbach and J. Caro, *Angew. Chem.*, 2010, **122**, 5078–5081; c) R. Makiura, S. Motoyama, Y. Umemura, H. Yamanaka, O. Sakata and H. Kitagawa, *Nat. Mater.*, 2010, **9**, 565–571; d) S. Motoyama, R. Makiura, O. Sakata and H. Kitagawa, *J. Am. Chem. Soc.*, 2011, **133**, 5640–5643; e) J.-L. Zhuang, D. Ar, X.-J. Yu, J.-X. Liu and A. Terfort, *Adv. Mater.*, 2013, **25**, 4631–4635; f) R. Ameloot, L. Stappers, J. Fransaer, L. Alaerts, B. F. Sels and D. E. De Vos, *Chem. Mater.*, 2009, **21**, 2580–2582; g) R. Ameloot, L. Pandey, M. Van der Auweraer, L. Alaerts, B. F. Sels and D. E. De Vos, *Chem. Commun.*, 2010, **46**, 3735–3737; h) K. Khaletskaya, S. Turner, M. Tu, S. Wannapaiboon, A. Schneemann, R. Meyer, A. Ludwig, G. van Tendeloo and R. A. Fischer, *Adv. Funct. Mater.*, 2014, **24**, 4804–4811; i) M. Tu, S. Wannapaiboon, K. Khaletskaya, R. A. Fischer, *Adv. Funct. Mater.*, 2015, **25**, 4470–4479.

- 9 O. Shekhah, H. Wang, S. Kowarik, F. Schreiber, M. Paulus, M. Tolan, C. Sternemann, F. Evers, D. Zacher, R. A. Fischer and C. Wöll, *J. Am. Chem. Soc.*, 2007, **129**, 15118–15119.
- 10 P. Falcaro, R. Ricco, C. M. Doherty, K. Liang, A. J. Hill and M. J. Styles, *Chem. Soc. Rev.*, 2014, **43**, 5513–5560.
- 11 a) P. Falcaro, A. J. Hill, K. M. Nairn, J. Jasieniak, J. I. Mardel, T. J. Bastow, S. C. Mayo, M. Gimona, D. Gomez, H. J. Whitfield, R. Riccò, A. Patelli, B. Marmiroli, H. Amenitsch, T. Colson, L. Villanova and D. Buso, *Nat Commun*, 2011, **2**, 237; b) R. Ameloot, E. Gobechiya, H. Uji-i, J. A. Martens, J. Hofkens, L. Alaerts, B. F. Sels and D. E. De Vos, *Adv. Mater.*, 2010, **22**, 2685–2688; c) I. Stassen, N. Campagnol, J. Fransaer, P. Vereecken, D. E. De Vos and R. Ameloot, *CrystEngComm*, 2013, **15**, 9308–9311; d) I. Stassen, M. Styles, T. van Assche, N. Campagnol, J. Fransaer, J. Denayer, J.-C. Tan, P. Falcaro, D. E. De Vos and R. Ameloot, *Chem. Mater.*, 2015, **27**, 1801–1807; e) K. Okada, R. Ricco, Y. Tokudome, M. J. Styles, A. J. Hill, M. Takahashi and P. Falcaro, *Adv. Funct. Mater.*, 2014, **24**, 1969–1977; f) T. Toyao, K. Liang, K. Okada, R. Ricco, M. J. Styles, Y. Tokudome, Y. Horiuchi, A. J. Hill, M. Takahashi, M. Matsuoka and P. Falcaro, *Inorg. Chem. Front.*, 2015, **2**, 434–441; g) J. Reboul, S. Furukawa, N. Horike, M. Tsotsalas, K. Hirai, H. Uehara, M. Kondo, N. Louvain, O. Sakata and S. Kitagawa, *Nat Mater*, 2012, **11**, 717–723.
- 12 a) H. Gliemann and C. Wöll, *Materials Today*, 2012, **15**, 110–116; b) V. Stavila, J. Volponi, A. M. Katzenmeyer, M. C. Dixon and M. D. Allendorf, *Chem. Sci.*, 2012, **3**, 1531–1540; c) M. C. So, S. Jin, H.-J. Son, G. P. Wiederrecht, O. K. Farha and J. T. Hupp, *J. Am. Chem. Soc.*, 2013, **135**, 15698–15701.
- 13 A. Bétard, S. Wannapaiboon and R. A. Fischer, *Chem. Commun.*, 2012, **48**, 10493–10495.
- 14 a) M. Tu, S. Wannapaiboon and R. A. Fischer, *Inorg. Chem. Front.*, 2014, **1**, 442–463; b) L. Heinke, M. Tu, S. Wannapaiboon, R. A. Fischer and C. Wöll, *Microporous and Mesoporous Materials*, DOI:10.1016/j.micromeso.2015.03.018.
- 15 a) K. Hirai, S. Furukawa, M. Kondo, H. Uehara, O. Sakata and S. Kitagawa, *Angew. Chem. Int. Ed.*, 2011, **50**, 8057–8061; b) K. Hirai, S. Furukawa, M. Kondo, M. Meilikhov, Y. Sakata, O. Sakata and S. Kitagawa, *Chem. Commun.*, 2012, **48**, 6472–6474.
- 16 a) S. Furukawa, K. Hirai, K. Nakagawa, Y. Takashima, R. Matsuda, T. Tsuruoka, M. Kondo, R. Haruki, D. Tanaka, H. Sakamoto, S. Shimomura, O. Sakata and S. Kitagawa, *Angew. Chem. Int. Ed.*, 2009, **48**, 1766–1770; b) K. Koh, A. G. Wong-Foy and A. J. Matzger, *Chem. Commun.*, 2009, 6162–6164.
- 17 S. Furukawa, K. Hirai, Y. Takashima, K. Nakagawa, M. Kondo, T. Tsuruoka, O. Sakata and S. Kitagawa, *Chem. Commun.*, 2009, 5097–5099.
- 18 D. Zacher, K. Yusenko, A. Bétard, S. Henke, M. Molon, T. Ladnorg, O. Shekhah, B. Schüpbach, T. de los Arcos, M. Krasnopolski, M. Meilikhov, J. Winter, A. Terfort, C. Wöll and R. A. Fischer, *Chem. Eur. J.*, 2011, **17**, 1448–1455.
- 19 O. Shekhah, K. Hirai, H. Wang, H. Uehara, M. Kondo, S. Diring, D. Zacher, R. A. Fischer, O. Sakata, S. Kitagawa, S. Furukawa and C. Wöll, *Dalton Trans*, 2011, **40**, 4954–4958.
- 20 B. Liu, M. Tu, D. Zacher and R. A. Fischer, *Adv. Funct. Mater.*, 2013, **23**, 3790–3798.
- 21 Z. Wang, J. Liu, B. Lukose, Z. Gu, P. G. Weidler, H. Gliemann, T. Heine and C. Wöll, *Nano Lett*, 2014, **14**, 1526–1529.
- 22 M. Tu and R. A. Fischer, *J. Mater. Chem. A*, 2014, **2**, 2018–2022.
- 23 M. Meilikhov, S. Furukawa, K. Hirai, R. A. Fischer and S. Kitagawa, *Angew. Chem. Int. Ed.*, 2013, **52**, 341–345.
- 24 M. Tu, S. Wannapaiboon and R. A. Fischer, *Dalton Trans*, 2013, **42**, 16029–16035.
- 25 L. Heinke, M. Cakici, M. Dommaschk, S. Grosjean, R. Herges, S. Bräse and C. Wöll, *ACS Nano*, 2014, **8**, 1463–1467.
- 26 C. Montoro, F. Linares, E. Q. Procopio, I. Senkovska, S. Kaskel, S. Galli, N. Masciocchi, E. Barea and J. A. R. Navarro, *J. Am. Chem. Soc.*, 2011, **133**, 11888–11891.
- 27 S. Wannapaiboon, M. Tu and R. A. Fischer, *Adv. Funct. Mater.*, 2014, **24**, 2696–2705.
- 28 G. Sauerbrey, *Z. Phys.*, 1959, **155**, 206–222.
- 29 There is a deviation of the deposited amount of the same MOF film (e.g DM) in different experiments. It could be attributed to the non-self-terminated “layer-by-layer” growth mechanism of these MOF films under this chosen LPE condition (Fig. S4, supplementary information) as well as the quality of the functionalised substrate.
- 30 However, the overvalued methanol adsorbed amount in the DE(10)-on-DM(20) film is observed due to the very low amount of DE shell component in the heterostructured film (featuring rather smooth facets of cubic MOF particles akin to the homostructured DM film, Fig. S9C).
- 31 A deviation at the end of the curve of the methanol adsorption in the presence of 45% P/P₀ of isopropanol (orange curve, Fig. 4A) from the single-component methanol adsorption isotherm can be explained by the surface condensation phenomena due to the near total saturation of alcohol vapour molecules in the gas flow.



Size selective adsorption of alcohols and molecular recognition of methanol over water are observed in the heterostructured $[\text{Zn}_4\text{O}(3,5\text{-dialkylcarboxypyrazolate})_3]_n$ thin films.